Tellus (2008), 60A, 372–383
Printed in Singapore. All rights reserved

TELLUS

'Explosive' meridional migration of cyclones and anticyclones

By DORON NOF*, *Department of Oceanography and Geophysical Fluid Dynamics Institute, Florida State University (FSU), Tallahassee, FL 32306, USA and Stephen Van Gorder, Department of Oceanography, Florida State University (FSU), Tallahassee, FL 32306, USA*

(Manuscript received 22 May 2007; in final form 21 November 2007)

ABSTRACT

We examine the very rapid meridional migration of barotropic eddies and show that the main balance of forces is between the meridional β-induced force and the opposing form-drag generated by the flow surrounding the rapidly moving eddy. The solution is constructed by assuming that, as the flow around a solid cylinder, the flow surrounding the eddy detaches from the eddy downstream.

We find the migration speed to be $(3\pi\beta V_m/5)^{1/2} r_m$, where V_m is the maximum orbital eddy speed and r_m is the radius where the maximum speed occurs. It is typically an order of magnitude faster than the classical westward speed induced by the baroclinic component ($\beta {r_m}^2$). The above formula gives values that are within 30–50% of the speeds measured in both our own numerical experiments, numerical experiments conducted by others, as well laboratory experiments (conducted by others).

We suggest that it is the barotropic component that very rapidly (10 km d^{-1}) pulls young Agulhas rings towards the equator. Poleward propagating cyclones are not very common but, during POLYMODE, an extremely rapidly propagating cyclone was observed in the North Atlantic. It is speculated here that its rapid propagation was also due to a barotropic component.

1. Introduction

Numerous oceanic observations as well as numerical and analytical models show the tendency of northern hemisphere upper ocean anticyclones (cyclones) to drift to the southwest (northwest) at a rate of about a kilometre per day (e.g. Robinson, 1983; Flierl, 1987; for reviews). Traditionally, the westward component of the drift has been attributed to β (the familiar variation of the Coriolis parameter with latitude) whereas the meridional component has been attributed to the associated radiation of energy from the light eddy to the surrounding and underlying heavier fluid. The logic behind this is that, when the orbital speed of anticyclones (cyclones) slows down due to the radiation of energy (rather than frictional decay), the now-less-energetic eddies tend to migrate towards the equator (poles) because this is where they can spin slower and yet maintain their original potential vorticity. With this conceptual picture, all eddies would ultimately reach their so-called 'latitude-of-rest' where they can no longer spin at all because all of their energy has been radiated away. (In reality, eddies collide with the oceans meridional boundaries much before this happens.)

Various numerical simulations display meridional drifts associated with the above processes (e.g. Mied and Liendeman, 1979) and so does the analytical solution for a light lens embedded in an extremely deep slightly heavier fluid on a β-plane (Flierl, 1984). However, since in these oceanic processes the tendency of the eddies to drift westward is the main aspect of their migration and, since the meridional speed is a mere secondary response to this tendency, the associated meridional speeds are relatively small (a few kilometres per day), certainly not much larger than the westward speeds that created them in the first place. Although many oceanic observations do agree with these estimates, some clearly suggest that other processes must also be at play on some occasions because the meridional speeds are sometimes much faster than the typical westward speeds.

For example, very young Agulhas rings are frequently observed to migrate towards the NNW at a rate of as much as 10–15 km d^{-1} (see Fig. 1a, Byrne et al., 1995; Schouten et al., 2000), and during POLYMODE (Fig. 1b), a small cyclone was observed to propagate northward at a speed as high as 5 km d^{-1} or more (Kamenkovich et al., 1986). Both of these speeds are an order of magnitude larger than the typical westward speed (roughly a kilometre per day or less). Here, we shall suggest

*Correspondence.
email: nof@ocean.fsu.edu
DOI: 10.1111/j.1600-0870.2007.00297.x

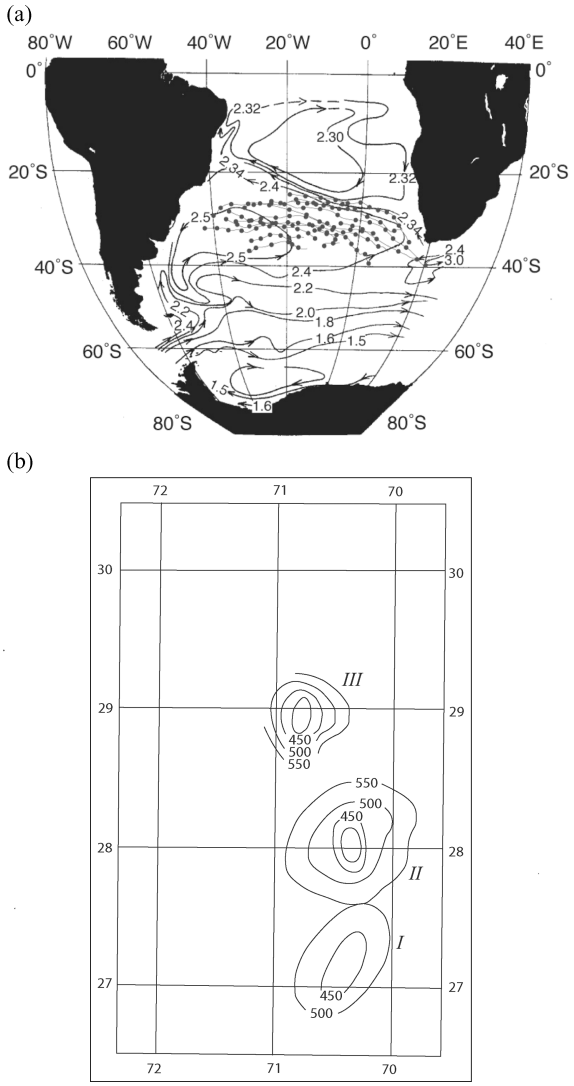

Fig. 1. (Top panel): Path of typical Agulhas rings. Steric anomaly at 500 dbar is contoured. The tracks are smoothed from estimates of the eddy centre, with shapes at evenly spaced time intervals of 34 d. Adapted from Byrne et al. (1995). Note that, initially, the rings drift fast to the NNW or NW. After about 100 d, their migration rate slows down considerably and their migration path becomes more and more zonal. We argue that the fast northward component (roughly 10 km d^{-1}) is due . (Bottom panel): Successive positions of a single cyclonic eddy in the POLYMODE region on (I) December 27–30, 1977, (II) January 17–19, 1978 and (III) February 9–10, 1978 (adapted from Kamenkovich et al., 1986 who credit Ivanov and Paramonov, 1980 for the plot). The contours represent the depth isolines (in m) of the 15 °C isothermal surface. (Larger orbital speeds and larger migration rates at a different orientation were observed after the shown periods. This suggests that, in the end of February, the eddy probably interacted with another feature.) During the shown period the eddy moved northward at the approximate rate of 5 km d^{-1}. The eddy appears to have intensified during the shown period (instead of decaying) but this may simply be due to the sampling and contouring issues which are not given in detail in Kamenkovich et al. (1986).

that, on those occasions that the meridional speeds are high, the eddies contain a strong barotropic component extending all the way from the surface to the ocean bottom. We term these very fast migrations 'explosive' in order to distinguish them from the much slower 'fast migrations' or 'rapid waves' terms frequently used to describe the recent observations of equatorial Rossby waves in the Pacific which travel twice as fast as the theoretically predicted Rossby waves speed (see e.g. Dewar and Morris, 2000; Killworth and Blundell, 2004; Paldor et al., 2007). Also, the term 'explosive' adequately describes the very temporary nature of the barotopic migrations that decay within 50–100 d.

1.1. Background

1.1.1. Observational background. Although there is no total agreement on whether Agulhas rings are formed by the retroflection itself (Pichevin et al., 1999) or some still-unknown instability, it is clear that they are not formed locally by the classical meander-like instability of zonal jets. The presence of a strong barotropic component (with speeds up to 0.2 m s^{-1} and higher) in relatively young Agulhas rings has been repeatedly suggested for decades (e.g. McCartney and Woodgate-Jones, 1991; Olson and Evans, 1985; Clement and Gordon, 1995; Witter and Gordon, 1999; Kamenkovich et al., 1996). When they are young ($\leq$100 d), the rings drift very rapidly ($\sim$10 km d^{-1}) to the NNW (or NW) but their migration rate gradually slows down and their orientation gradually adjusts to become more and more towards the west so that, ultimately, their drift is slow ($\sim$1 km d^{-1}) and purely towards the west. The initial fast northward migration is frequently attributed to surrounding advective flows. However, it is not at all a trivial matter to estimate the momentum introduced by (both old and new) Agulhas rings to the Southeastern Atlantic and determine what fraction of the ring movement is due to an environmental flow and what is due to its very own self-propulsion.

Some calculations simply take the difference between the migration speed of each ring and the speed of its immediate environment to be the contributed anomaly. We argue that this grossly underestimates the ring's own speed because the volume flux of the rings (which is, say, 10 *Sv*) is so large that the whole Southeastern Atlantic is full of remnants from old rings that also moved to the north. To correctly do the estimate, one needs to consider the motion that the Southeastern Atlantic would have had in the *absence* of the rings. It is hard to tell for sure what that would be but the northward Sverdrup transport is a plausible candidate—it is roughly 1 km d^{-1}, an order of magnitude smaller that the speeds of interest here. We shall suggest here that the observed high meridional migration speeds correspond to barotropically induced self-propulsion, not the much weaker Sverdrup flows. As far as the POLYMODE cyclone is concerned, there is really no evidence for the presence (or absence) of a barotropic component and, consequently, our suggestion that its very rapid meridional migration was due to a barotropic component should be regarded as speculative.

1.1.2. Theoretical background. We shall show that a barotropic component forces intense cyclones poleward and intense anticyclones towards the equator because these are the directions that the β-induced force is pointing to. In this scenario, the meridional β-induced force is balanced by an opposing form-drag associated with pressure exerted by the surrounding fluid flowing around the barotropic eddy. (The terms 'lift' and 'drag', which are very familiar to fluid dynamicists but not necessarily to oceanographers and meteorologists, will be used throughout. The reader who is unfamiliar with these ideas is referred to any fundamental fluid dynamics reference book.) We shall neglect the effects of 'lift', that is, the sideway pressure exerted by the environmental fluid in a direction *perpendicular* to the direction of migration on the ground that such lift requires frictional transmission of energy between the eddy and the environmental fluid. Note that the recognition that barotropic cyclones (anticyclones) may move towards the equator (poles) was originally made by Rossby (1948) who was the first to realize that all eddies are subject to a meridional β-induced force. He stopped short, however, of deriving any migratory speeds or addressing the meridional balance of driving forces.

Dewar and Galliard (1994) also recognized the importance of a barotropic component in Agulhas rings and illustrated that, due to mutual advection (associated with the requirement that the baroclinic, and barotropic component be off-centred), a barotropic component can force those rings to move rapidly in any direction. While very useful, this mechanism weakness is that it does not have a preferred direction of migration and, hence, it does not explain the observed Agulhas rings migration, which clearly has a preferred orientation (NNW). Similarly, although bottom togography is definitely an important aspect of Agulhas rings dynamics (see e.g. Drijfhout, 2003; Van Aken et al., 2003), its role in the rapid NNW migration is questionable because the orientation of the topography varies wildly within the rings' initial meridional path. For related aspects of eddies and topography, the reader is referred to Nycander and LaCasce (2004) and the references given their in.

We shall argue that the observed meridional migration is due to a balance between the β-induced force and form-drag, a very different process than the mutual-advection process of off-centred eddies or bottom topography. The force balance of our intense, non-radiating eddy is also very different from the radiation and eddy–eddy interaction issues considered by Reznik et al., (2000), Korotaev (1997), DeMaria (1985) and Firing and Beardsley (1978). By and large, these studies address migratory speeds much smaller than ours. As a result of the different force balance, our speeds are an order of magnitude larger than that of the so-called β gyres, as well as an order of magnitude greater than those usually associated with Rossby waves [(:$o(\beta r_{\mathrm{m}}^2)$, where r_{m} is the radius of maximum speed].

One of the most closely related studies to our work is that of Smith (1993), who analysed the results of all previous numerical experiments simulating hurricanes, and empirically (i.e. without addressing the associated dynamics) came up with a formula almost identical to ours. The vortices in many of the models that he analysed were not intense and we shall see that it is due to this lack of intensity that they had a westward drift component as strong as the meridional. His formula is, nevertheless, very close to ours with the only difference that the coefficient $(3\pi/5)^{1/2}$ is replaced by the numerically determined coefficient of about 0.6 giving meridional speeds that are about half of ours. A simple scaling argument (which will be addressed later) shows that the 30–50% difference between the two speeds is due to frictional effects that are not present in either our analytical model or the ocean and yet are present in both his and our numerics. Another very relevant study is that of Flór and Eames (2002, FE, hereafter) who carefully and meticulously measured the speeds of cyclones in the laboratory and found them to be fairly close to ours. We shall return to those two studies and their implications later. Before proceeding and describing the layout of this document, we shall briefly discuss the differences and similarities of drag and lift, both of which are critical to our study.

1.2. Drag-versus-lift

Both drag and lift result from asymmetrical pressure fields around the vortex-cylinder. A drag is, by definition, a pressure force in the direction *opposing* the migration whereas a lift is a sideway pressure force in the direction *perpendicular* to the migration. For many flows both forces are present and often the two are of the same order. This is certainly the case for the classical non-rotating flow around a spinning cylinder with a separation downstream. The separation causes an asymmetry in the flow direction (i.e. the downstream and upstream fields relative to the cylinder are not the same) whereas the spin introduces asymmetries in the direction perpendicular to the flow. A clockwise (counter-clockwise) spin adds to the speed on the left-(right-)hand one side of the cylinder and subtracts from the speed on the right-(left-)hand side (looking downstream). In this case, the detachment causes the drag whereas the spin causes the lift. Without detachment, there is no drag and, without the spin, there is no lift. Note that the lift mentioned here is sometimes referred to as the 'Magnus effect'.

There are many flows where only one of the two forces is present. For instance, for obvious economical reasons, aeronautical engineers attempt to design (asymmetrical) wings that maximize the lift and yet minimize the drag. On the other hand, when air bubbles rise in an otherwise still liquid or solid spheres fall in a fluid, the flow around the object is symmetrical in the direction perpendicular to the rise (or fall) and *asymmetrical* in the direction of the rise. As a result, there is only drag and no 'lift' so the objects rise (or fall) exactly in the vertical direction with no movements to the sides. Often these objects reach the so-called 'terminal velocity' whereby the gravitational force or buoyancy force balances the drag. (We shall see shortly that this conceptual balance is analogous to our proposed balance where

gravity is replaced by the β-force.) By contrast, when an autumn leaf falls from a tree (in an otherwise still air) it moves sideways as well as downward because its shape is asymmetrical in both directions so that a horizontal pressure force (lift) is exerted on it.

For our barotropic vortex-cylinder we shall assume that there is drag but no lift. This means that the flow is taken to be symmetrical in the cross-drift direction but asymmetrical in the drift direction. The logic behind this assumption is that, in order to produce lift, the vortex-cylinder must somehow transmit its very own orbital motions to the exterior fluid so that the environmental fluid will speed up on one side and slow down on the other. In the solid cylinder case, the orbital speed along the rim is large and is directly superimposed on the outer fluid in the presence of friction. This is why lift is produced. In the vortex case, on the other hand, the orbital speed along the rim is usually zero so no motion can be easily transmitted from the vortex to the environmental fluid. This is why there should be almost no-lift in the vortex case. It will become clear later that this no-lift assumption implies small zonal migrations, a condition that, for intense eddies, is satisfied by both our numerics and the FE experiments.

As correctly pointed out by FE, a lift produces a zonal movement, as opposed to the meridional movement that is caused by the β-force. Although FE adequately attributed the zonal movement to the lift, their estimate of the lift appears to be in disagreement with both their own experiments and with the expected velocity scales. In contrast to their calculation, their laboratory produced eddies did not accelerate in the zonal direction during the course of their runs. Also, as mentioned above, the assumption that the maximum orbital speed is directly transmitted to the environmental fluid grossly overestimates the actual transmitted speed (by at least an order of magnitude) because the vortex orbital speed usually goes to zero near the outer edge.

We shall consider an intense barotropic vortex with a parabolic velocity profile (Fig. 2) within the context of the shallow water equations on a β-plane. Since the horizontal scale of these eddies is roughly 10–100 km, which is much smaller than the barotropic Rossby radius (roughly 2000 km), we shall argue that the flow surrounding the vortices is governed by the zero-amplitude limit of the inviscid potential vorticity equation. We shall also argue that, because the Rossby waves and β-gyres speed (βr^2) is an order of magnitude smaller than our soon-to-be-derived migration rate [$(\beta V)^{1/2} r$], β can be taken to be zero *out side* the vortex (to first order). Taking the potential vorticity to be f_0/H we find that, under the above conditions, the exterior is governed by the Laplace equation (i.e. outside the vortex, the flow is taken to be a potential flow). As mentioned, the familiar Magnus effect will be neglected on the ground that only small speeds are transmitted from the eddy to the surrounding fluid so that it produces velocities an order of magnitude smaller than ours.

In Section 3, we show that our vortex meridional drift is analogous to the 'terminal velocity' of falling or rising objects whereby buoyancy or gravity balances the form-drag and the lift is zero.

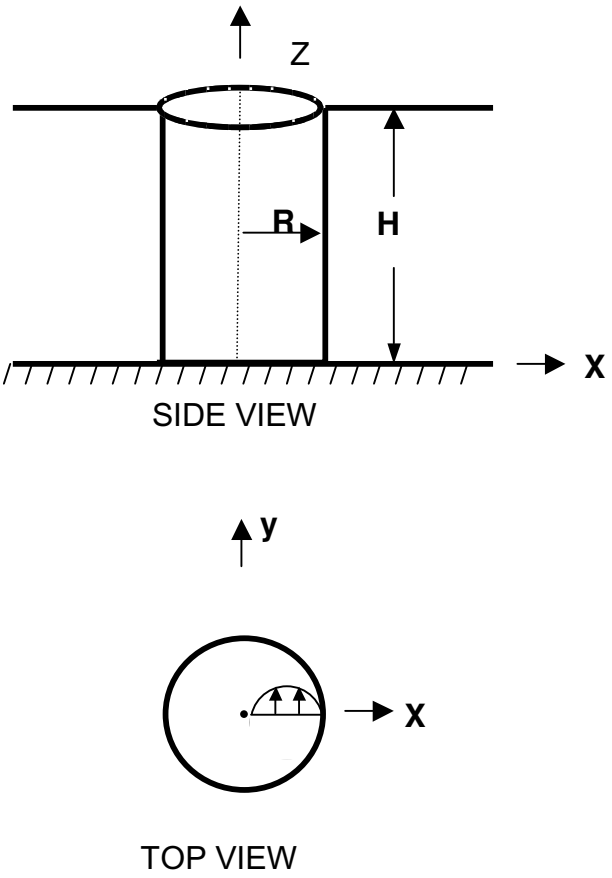

Fig. 2. The adopted simplified structure of the vortices. The orbital velocity profile is parabolic with the velocity reaching a maximum at $R/2$ and vanishing along the edge (R).

Here, the main vortex force balance is between the β-force induced by the intense vortex ($\beta \int\int \psi \, dx \, dy$, where ψ is the stream function and the remaining notation is conventional) and a form-drag exerted by the fluid surrounding the vortex. This form-drag is similar to that exerted on a stationary solid cylinder by an (upstream uniform) flow that separates from the edges downstream creating low-pressure in the lee of the cylinder (relative to the high-pressure on the upstream side of the cylinder). The flow surrounding a column of a bridge often displays these aspects. We shall see that this balance implies a meridional drift with the scale $(\beta V_{\max})^{1/2} r_{\max}$, where $V_{\max}$ is the vortex maximum orbital speed and $r_{\max}$ is the radius at which the maximum speed occurs.

The ratio between this meridional speed and the Rossby wave speed is $(V_{\max}/\beta r^2_{\max})^{1/2}$, which, for typical ocean eddies, is between 10 and 100. Hence, we shall neglect the westward speed as well as the β-gyres, and derive an analytical solution for a purely meridional drift. Furthermore, to obtain the drift lower-bound, we shall assume that the detachment occurs at the eastern and westernmost points A and B (Fig. 3) so that the drag-force

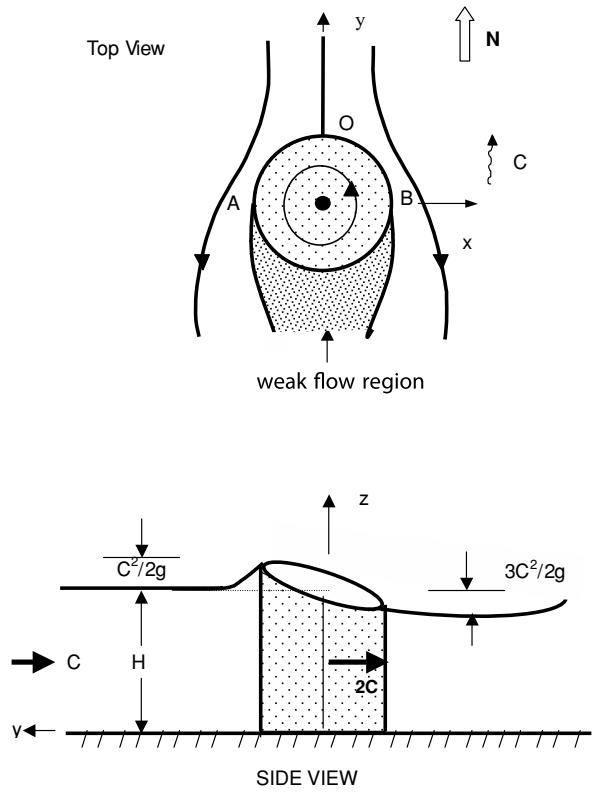

Fig. 3. Schematic diagram of the northward propagating (southern hemisphere) anticyclone (Agulhas) or the (northern hemisphere) cyclone in a coordinated system travelling with the vortex at the speed C. The barotropic eddy scale (∼100 km) is much smaller than the barotropic Rossby radius (∼2000 km) so the upstream flow surrounding the vortex is viewed as inviscid potential flow. To estimate the maximum drag on the vortex, it is assumed that this flow separates from the vortex western and eastern most edges (A and B) and that the flow is very weak in the lee (shaded region). The sea level differences noted were obtained by applying the Bernoulli along the streamline originating upstream at infinity ($x = 0$, $y \to \infty$) and passing through the stagnation point O, and the detachment points A and B.

exerted on the vortex is maximized. After obtaining the analytical solution in this manner, we shall proceed and conduct a series of numerical experiments (Section 4). The final outcome of these experiments is a reasonable agreement between the analytics and numerics, with the analytically predicted speed being almost twice as much as the numerical speed. A simple scaling shows that the difference between the two is mostly due to friction. As should be the case, our numerical results are in a better agreement with earlier numerical experiments as well as with the recent laboratory experiments of FE (because friction is present in all of them).

Just like in all numerical experiments of this sort, to keep the eddies (whose vorticity changes sign as one proceeds from the centre to the rim) from breaking up, a non-negligible horizontal frictional coefficient had to be used. Consequently, by the time that the eddy adjusts to the presence of β (about 60–70 d), the orbital velocity has already slowed down. Hence, the supposedly large ratio of the meridional to the zonal speed $(V_{\max}/\beta {r_{\max}}^2)^{1/2}$ which is 10–100 in the ocean and of order ten in the beginning of the experiments, has been reduced to about three. This is still larger than unity but means that terms that have been neglected as small in the analytics (and are probably small in the ocean) are approximately 30% of the other terms in the numerics. This is still very reasonable and the numerical simulations display the same main balance that the analytics. A comparison of the analytics to the drifts observed in the ocean is presented in Section 5 where the results are summarized and discussed.

1.3. Outline

2. Formulation

On an f-plane, the steady barotropic eddy (Fig. 2) is assumed to have a parabolic orbital velocity profile,

$$V_\theta = -2R_0 f_0 r(R - r)/R, \tag{1}$$

where R_0 is the Rossby number, and R is the eddy radius. This speed vanishes at the centre and rim and has a maximum at $R/2$, where it has the value of $R_0 f_0 R/2$. The region outside this f-plane vortex is taken to be at rest. The eddy is barotropically stable inside because it does not involve an inflection point within the vortex itself. Unavoidably, this is incorrect along the eddy edge ($r = R$), where there is an inflection point causing a local instability. (In the numerical experiments, which will be described later, viscosity damps this instability.)

With our formulation, the β-plane vortex is drifting in the north-south direction at the speed of the order of $(\beta V_{\max})^{1/2} r_{\max}$, which is roughly 10 cm/s. This scale is obtained from the soon-to-be-derived balance,

$$\beta \int\int \psi \,\mathrm{d}x\,\mathrm{d}y : C^2 r_{\max} H, \tag{2}$$

where C is the migration rate. Relation (2) corresponds to a β-force (left-hand side) balanced by a form-drag (right-hand side) whose estimate is obtained by applying the Bernoulli integral to the splitting streamline associated with point 0 (Fig. 3). In a coordinate system moving with the eddy-cylinder, the far upstream region appears to be moving towards the eddy at $-C$ so that, by Bernoulli, the water at the stagnation point O is $C^2/2g$ higher than upstream. With the aid of the potential flow solution that will be employed later, we shall see that the speed at the detachment points A and B is $2C$ so that the wake level is $3C^2/2g$ lower than the upstream level. Note that the presence of H in eq. (2) is due to the expression for the hydrostatic pressure on both the upstream and the lee side.

As mentioned, the ratio of the above speed to the familiar Rossby wave speed $(\beta r_{\max}^2)$ is, $(V_{\max}/\beta r_{\max}^2)^{1/2}$, which is typically of order ten or so. Namely, while the meridional migration rate, $(\beta V_{\max})^{1/2} r_{\max}$, is still much smaller than the orbital speed

[because the ratio between the two speeds is $(\beta r_{\max}/f_0)^{1/2}$ which is typically 0.1], it is, at the same time, much faster than the Rossby wave speed. Note that, as expected, for the ocean, the ratio of the right-hand side of (2) to the bottom stress ($C_D C V_{\max} r^2{}_{\max}$, where C_D is a non-dimensional bottom drag-coefficient whose value is approximately 2×10^{-3}) is about ten, that is, the form-drag is much greater than the oceanic bottom stress. Also, the form-drag is much larger than the side frictional effects induced by horizontal friction, which attempts to slow the eddy's migration down. To see this recall that the ratio of the form-drag (which is an inertial effect induced by friction) to the actual frictional force (that is acting like brakes on the eddy rim) is the Reynold's number based on the migration speed C, the horizontal viscosity, and the eddy radius.

Even for very slow migration rates and as high oceanic viscosity coefficient that one wishes to consider for our situation, this number is at least an order of magnitude larger than unity (in both the ocean and the numerical experiments), indicating that this friction is much smaller than the terms considered in eq. (2). For example, taking the migration rate to be 0.1 m s^{-1}, an eddy radius of merely 10 km and an oceanic horizontal eddy viscosity as high as 100 m^2 s^{-1}, still gives a Reynolds number of 10. However, in contrast to this almost-no-friction *oceanic* situation, the Reynolds number in the numerical experiments is (unavoidably) merely *three* implying an error of approximately 30%. This means that friction has a much larger role in the numerics than it does in the ocean.

To obtain the solution, we shall integrate the y-momentum equation over the vortex, that is, over the area confined by the closed streamline separating the vortex from the surrounding fluid. It is difficult to identify such a streamline in reality (i.e. in both the numerical experiments and the ocean) because the eddy's fluid along the edge constantly mixes with the environmental fluid. In the idealized limit of no-mixing, however, such a separated streamline and an associated weak flow region in the lee of the vortex should exist as, otherwise, the β-force will forever accelerate the eddy (in the meridional direction). Such acceleration is not observed in the ocean, laboratory, or the numerics indicating that a terminal drift velocity is reached.

Since the meridional drift, $(\beta V_{\max})^{1/2} r_{\max}$, is much slower than the orbital speed, $f_0 r_{\max}$, we shall view the problem as a slowly varying problem. Namely, in a coordinate system slowly moving meridionally with the eddy's centre (at the speed of the eddy), the problem will appear to be steady so that all the terms that explicitly involve time can be ignored. Recall that, as mentioned, the westward drift, $\beta r_{\max}{}^2$, is still much smaller than the meridional drift (which, by itself, is smaller than the orbital speed) and, consequently, the term which generates it outside the vortex (βy) will be totally neglected as well. In the ocean, the three speeds have indeed three different orders of magnitude. The orbital speed is $\sim$0(1 ms^{-1}), the smaller meridional drift is $\sim$0(0.1 ms^{-1}), and the still smaller westward speed is $\sim$0(0.01 ms^{-1}). We shall see later that the numerics represent an approximate duplication of this velocity-ratio situation. However, it takes the numerical eddy time to adjust to β and, by the time that this adjustment is achieved, the orbital speed ($V_{\max}$) has been reduced and the eddy's size ($r_{\max}$) increased so that the westward speed is about a third of the meridional speed.

3. Solution

3.1. Main balance

We begin by integrating the steady y-momentum equation over the drifting vortex,

$$\iint [\partial(huv)/\partial x + \partial(hv^2)/\partial y]\,\mathrm{d}x\,\mathrm{d}y + \iint fuh\mathrm{d}x\,\mathrm{d}y = g\iint (H+\eta)\,\partial\eta/\partial y\mathrm{d}x\,\mathrm{d}y, \tag{3}$$

where in our conventional notation which is detailed in both the text and the Appendix, h is the total thickness, $(H+\eta)$, u and v the horizontal velocity components (in the meridionally moving coordinate system), H the undisturbed depth and η is the free surface displacement ($\ll H$). Note that the meridional migration speed C does not *explicitly* appear in (3) but it is an explicit part of the x-momentum equation (which will not be used because, as we shall shortly see, it is automatically satisfied). Converting the first surface integral to a contour integral and introducing the stream function,

$$\psi_y = -uh; \quad \psi_x = vh, \tag{4}$$

we obtain,

$$\oint huv\,\mathrm{d}y - \oint hv^2\mathrm{d}x + \iint \left[\beta\psi - \frac{\partial}{\partial y}(f\psi)\right]\mathrm{d}x\,\mathrm{d}y - g\oint H\eta\mathrm{d}x = 0 \tag{5}$$

where we neglected terms whose ratio to the retained terms is of (η/H), and the integration is done in a counter-clockwise manner. Our definition of the streamfunction, which involves the layer thickness (h), is somewhat different than that frequently used in barotropic models where the thickness is taken to be constant. Since the dynamics of the problem at hand involves sea surface variations, it is more appropriate to choose the form with varying h which is the more general definition.

Noting further that, along any streamline such as the closed streamline separating the vortex from the environmental fluid, $u\,\mathrm{d}y = v\,\mathrm{d}x$, and that, without any loss of generality, we can define ψ to be zero along this closed contour, (5) can be written as,

$$\beta\iint \psi\mathrm{d}x\,\mathrm{d}y = gH\oint \eta\mathrm{d}x, \tag{6}$$

which is our desired force balance. The left-hand side is the eddy-induced β-force [southward for an anticyclone ($\Psi > 0$) and northward for the cyclone ($\Psi < 0$)] and the right-hand side is the opposing form-drag resulting from a lower sea level in the lee. Recall that this balance of forces is in the direction of motion

(y). Rossby waves and β-gyres in the exterior can also contribute to these forces but, as mentioned, their contribution is neglected here because their speeds are an order of magnitude smaller than C.

Since the variations introduced by β are small (because $\beta R/f_0$ is small), the left-hand side of (6) will be computed by taking Ψ to be that of the radially symmetric f-plane eddy described by (1). The right hand side of (6) will be computed by assuming a detachment downstream and recalling that R, the eddy radius, is at least an order of magnitude smaller than the barotropic Rossby radius. Therefore, to first order, the flow surrounding our intense eddy is not affected by rotation, that is, it can be taken as the potential flow solution around a cylinder modified by a detachment downstream.

Next, we shall use the approximated Bernoulli integral (B) in the (approximately) steadily northward moving coordinate system,

$$\frac{q}{2}^2 + f_0 C x + g\eta = B(\psi), \tag{7}$$

where $q^2 = u^2 + v^2$, and B is the Bernoulli function. The contribution of β is neglected here on the ground that the Rossby waves speed is much smaller than C. The reader is referred to Nof (1983, 1985), where the derivation of the Bernoulli from the x and y momentum equations in a moving coordinate system with rotation is discussed in detail. Relation (7) states that the quantity, $q^2/2 + f_0 C x + g\eta$, is constant along a streamline (because ψ is a constant along a streamline). Note that both the Magnus-lift effect (which is later neglected here) and the form-drag (which is included here) are associated with the first term on the left-hand side of (7).

The second term on the left hand side is associated with the so-called 'planetary lift' discussed in Nof (1983, 1985). It represents the force resulting from a Coriolis-induced difference in elevation around the vortex. While very important for baroclinic eddies, it is of no consequence here as, for a barotropic fluid, it is exactly cancelled by the Coriolis force associated with the northward movement of the eddy. To see this, we integrate the pressure term ($g\eta$) expressed by (7) in y over the closed vortex boundary taking into account the flow surrounding the vortex. Since the posed problem is assumed to be symmetrical in x (i.e. values in $-x$ are identical to those in $+x$), the only term that is left from this integration (i.e. the only one that does not vanish) is the integral of the second term, $\oint f_0 C x \, \mathrm{d}y$, which represents the zonal force acting on the vortex. This force is just the migration rate times (minus) the eddy area, that is, the westward force exerted on the eddy by the environmental fluid. It is straightforward to show that, in this zonal direction, the integrated Coriolis force over the vortex interior is equal and opposite to the exterior force. To see this, one integrates the x-momentum equation over the vortex interior to get, $\iint f_0 C \mathrm{d}x \, \mathrm{d}y$, which exactly balances the 'planetary lift', $\oint f_0 C x \, \mathrm{d}y$. This barotropic cancellation of the planetary lift (to be distinguished from the neglect of the Magnus lift) and Coriolis is not new—it was first recognized by Rossby (1948) and is mentioned in passing in his original article (again without any derivation).

3.2. Form-drag

To calculate the form-drag (F_D), we will assume that, in a similar fashion to the flow surrounding a solid cylinder, the outside flow detaches from the eddy downstream. The idea behind this approach is that both a solid cylinder and an eddy correspond to a circular boundary through which there is no flow. The only obvious difference between the two is that, in the eddy case, the sea level is, of course, continuous across the circular boundary. Since the sea level does not enter the approximated vorticity equation (Laplace, in our case), there is no difference between the outside flow around a cylinder and that around the eddy.

The downstream detachment means that the velocities downstream are significantly smaller than those upstream so that, via Bernoulli (7), there is a pressure force opposing the β-force which pulls the eddy meridionally. To obtain the lower bound on the migration speed, we will assume that detachments occur at the easternmost and westernmost points (A and B in Fig. 3) so that the form-drag is maximized. Upstream (and only upstream) of AOB, the flow is taken to be the potential flow solution around a solid cylinder. [Acheson (1990) describes a similar approach for a slightly different form-drag calculation.] According to that solution, the stream function (in polar coordinates, r and θ, where θ is measured counter-clockwise from the x-axis) satisfying the boundary conditions,

$$\psi \to -Cr\cos\theta, \quad \text{at } r \to \infty \text{ and, } \psi = 0 \text{ at } r = R, \qquad 3.2.$$

is,

$$\psi = C(r - R^2/r)\cos\theta.$$

It corresponds to,

$$u_r = C(1 - R^2/r^2)\cos\theta, \quad \text{and } u_\theta = -C(1 + R^2/r^2)\cos\theta,$$

where u_r and u_θ are the radial and tangential velocities. Accordingly, the speed (q) along the vortex edge (i.e. the streamline separating the cylinder-vortex from the surrounding fluid, where $r = R$) is,

$$q = -2C\cos\theta, \tag{8}$$

where as mentioned, $\theta = 0$ along the positive x-axis. Recall that, when there is no detachment downstream, this potential flow is symmetrical with respect to both the x- and y-axes implying that there is no net force on the cylinder-eddy. This is the so-called d'Alembert Paradox.

Taking the flow downstream of the detachment points to be zero and considering Bernoulli (7), the form-drag (F_D) is found by integrating the pressure ($g\eta$) around the eddy (in x) to be,

$$F_D = gH \oint \eta \mathrm{d}x = HR \int_0^\pi (q^2/2)\sin\theta \, \mathrm{d}\theta = (4/3)\mathrm{HRC}^2. \tag{9}$$

Note that all the other terms in (7) vanish upon the integration and that F_D is always opposing the migration.

3.3. The β-force

The force pulling the vortex merdionally,F_β, is,

$$F_\beta = \beta \int_0^R \int_0^{2\pi} \psi r \, \mathrm{d}\theta \, \mathrm{d}r.$$

Using (1), one finds, after some straightforward algebra,

$$F_\beta = \frac{-2H\beta R_0 f_0}{R} \int_0^{2\pi} \int_0^R \left(R^3/6 - R\frac{r^2}{2} + \frac{r^3}{3} \right) r \, \mathrm{d}r \, \mathrm{d}\theta$$
$$= -\beta\pi H R_0 f_0 R^4/10. \quad (10)$$

It is positive (southward) in the northern hemisphere for an anticyclone ($R_0 > 0; f_0 > 0$) and negative for a cyclone.

3.4. Detailed solution

Combining (9) and (10) and carrying out the associated algebra, one ultimately finds our desired (surprisingly simple) migration formula,

$$C = \left(\frac{3\pi}{5} \beta V_{\max} \right)^{1/2} r_{\max}, \quad (11)$$

where C is the minimum poleward speed for a cyclone (and the minimum equatorward speed for an anticyclone), $V_{\max}$ is the absolute value of the maximum velocity ($R_0 f_0 R/2$) and $r_{\max}$ is the radius at which the velocity is a maximum ($R/2$ in our analysis).

In the next section, we shall compare our analytical solution to our own numerical runs, to other numerical runs as well as to the lab experiments of FE. We shall see that, while (11) compares reasonably well to the numerical values, numerical mixing blurs the separating streamline to the extent that the detachment points cannot be easily identified. (This is also noted in the laboratory experiments of FE.) As expected, both the numerical and the laboratory speeds are lower than the analytically predicted speeds (11) because numerical and laboratory friction slows down the migration. This is the case even though (11) is the minimum predicted speed, because (11) is the minimum for an *inviscid* migration (i.e. when $\upsilon \to 0$), not a frictional migration. It is estimated that our analytical speeds will be closer to the oceanic applications than either the numerics or the laboratory because both of these are dominated by friction.

4. Numerical simulations

We have used a single layer numerical model with a free surface (i.e. without the rigid lid approximation) that we adapted from the Black and Boudra original isopycnic model. The model has lateral Laplacian friction but no bottom and no vertical friction. We initialized it with a (10 km radius) stationary eddy with the previously discussed (stable) parabolic velocity profile (1). The numerical grid count was 101 × 101, $\Delta x = \Delta y = 1$ km, and $\Delta T = 0.54$ s.

We conducted a total of 40 experiments with varying viscosity and Rossby numbers in an attempt to avoid eddy breakup and yet keep the viscosity at a minimum. We ultimately focused on four experiments described in Table 1; one of them is shown in Fig. 4. (Since our analytically predicted speed was constantly adjusted during the experiment, showing the four experiments require four separate figures which we feel is unnecessary. The three that are not shown are almost indistinguishable from Fig. 4.) For each experiment, we measured the eddy centre radius and speed everyday, implying that each experiment provides about 50 valid data points. The centre of the eddy was identified as the point where the vorticity has its maximal value, whereas the radius is identified as the mean radius of the closed contour along which $\partial V_\theta / \partial r$ is a maximum. Although not really necessary, to make the plots easier to view, the centre position was filtered with an 11 d centred running mean whereas the drift speed was filtered with a 21 d mean. The changes that the eddy experience with time due to the numerical friction are shown in Fig. 5. The streamlines in the vortex lee (adjusted for the eddy translation) are shown in Fig. 6, the balance of forces in Fig. 7 and the eddy trajectory is shown in Fig. 8.

The run presented in Fig. 4 shows a reasonably good agreement between the predicted speed and the numerical speed after the eddy adjusts to the presence of β (day 70 or so). As expected, the figure displays a better agreement with the numerical results consolidated by Smith (1993) to his empirical formula (dashed-line) and to the laboratory experiments of FE for intense eddies

Table 1. Details of the primary four experiments

EXP number	Rossby number	Lateral viscosity, υ (m^2 s^{-1})	f_0 (Coriolis)	β	H
1	0.3	3			
2	1.0	9			
3	−0.3	3	10^{-4} s^{-1}	1.67×10^{-11} m^{-1}s^{-1}	3000 m
4	−1.0	9			

Note that the viscosity gives a decay time scale ($r_{\max}{}^2/\nu$) of 50–80 d implying that the analytically predicted speed needs to be adjusted throughout the experiment.

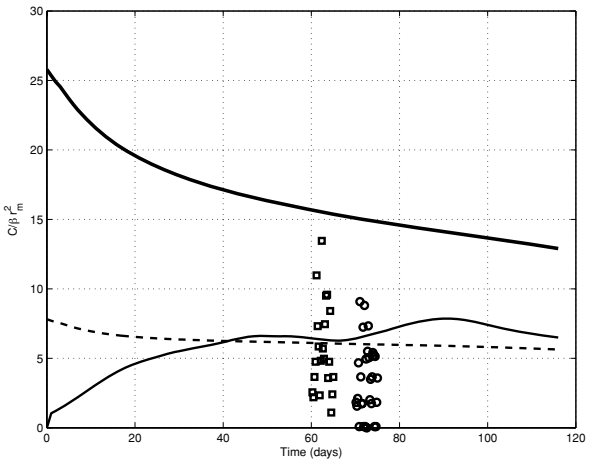

Fig. 4. The adjusted analytical drift (upper solid curve) and numerical (lower solid curve) meridional speed as a function of time for experiment no. 1. The adjustment of the analytical speed was made on the basis of both the numerically measured maximum speed and the radius. The dashed line is the empirically predicted speed of Smith (1993). The squares and circles are the results of the laboratory experiments of FE (their fig. 9a). Note that the experimental adjustment time $[(\beta R)^{-1}]$ is roughly 70 d so that the period that we need to focus on is the period between 70 and 115 d. For that period, there is very good agreement between our numerics, Smith (1994) empirical result and EF. The agreement between the theoretical and numerical values is also reasonable (∼50%) but this agreement is, of course, not as good as that between the two numerical simulations (Smith's and ours) and the laboratory experiments because of the presence of friction in both the numerics and the laboratory. As expected, the theoretical meridional speeds are higher than the numerical and laboratory speeds according to the scaling, $\nu/\beta\, r^3$. Note that the numerical measurements were done daily so each experiment corresponds to 50 or so data points.

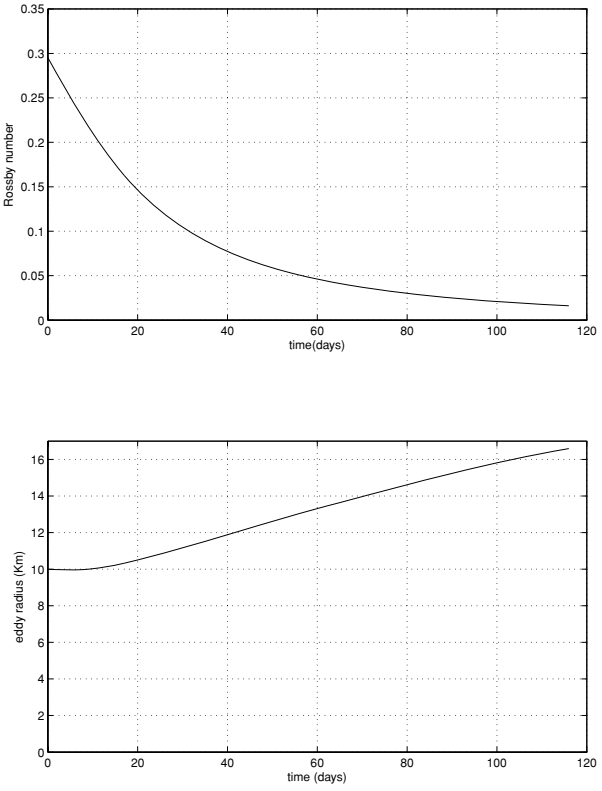

Fig. 5. The numerical decrease in Rossby number (upper panel) and the increase in eddy size (lower panel) as a function of time. Both reflect the effect of horizontal friction, which, due to numerical stability issues common for all numerical experiments of this nature (e.g. Simmons and Nof, 2002; Cherubin et al., 2006), could not be placed at less than 5–9 $m^2\ s^{-1}$ (corresponding to an acceptable diffusion speed of 1 cm s^{-1} or less).

(that did not break up) because all these experiments involve non-negligible friction. Squares correspond to the EF squares (shown in their fig. 9a) indicating a strong eddy whereas circles correspond to their circles indicating a still intense but somewhat weaker eddy. As expected, for intense eddies, the β-force is large so the meridional drift speed is large as well. In the same time, the lift is still relatively small because it is merely a function of the eddy orbital speed near the rim that is not strongly dependent of the eddy intensity and is supposedly very small in all cases. Hence, as schematically shown in Fig. 7, intense eddies are expected to move towards the north whereas weaker eddies are expected to move more towards the northwest (due to an increased relative importance of the lift).

As should be the case, both the laboratory speeds and the numerical speeds are lower than our analytically predicted speed because both contain frictional forces that are absent from our model. Despite the approximations made in the derivation of the analytical formula, and despite the presence of friction in the numerics, the two values are consistently within 30–50% of each other for a long period of time (50 d or so) during which numerous calculations were made. This is consistent with the estimate that the role friction in the numerics (relative to the β-force) is $\sim o(\nu/\beta r^3)$ giving that frictional forces could be as much as half of the β-force. Because of the unavoidable use of numerical friction that reduced the eddy intensity and, hence, increases the relative importance of the lift, the eddy meridional drift was merely three times as fast as the westward drift. While still larger than unity, this forced the eddy to migrate in the NNW direction rather than in the purely meridional direction (see Fig. 8, left-hand panel). Although this is not an ideal situation, it is an acceptable comparison. Fig. 8 (right-hand panel) clearly illustrates that the same NNW drift existed in the intense-eddies laboratory experiments of FE. While it is definitely possible to identify a region of very weak velocities at the lee of both the laboratory and numerical eddy (Fig. 6), because of a small but steady mixing of the eddy fluid with the environmental fluid, it is difficult to verify the detachment in the lee.

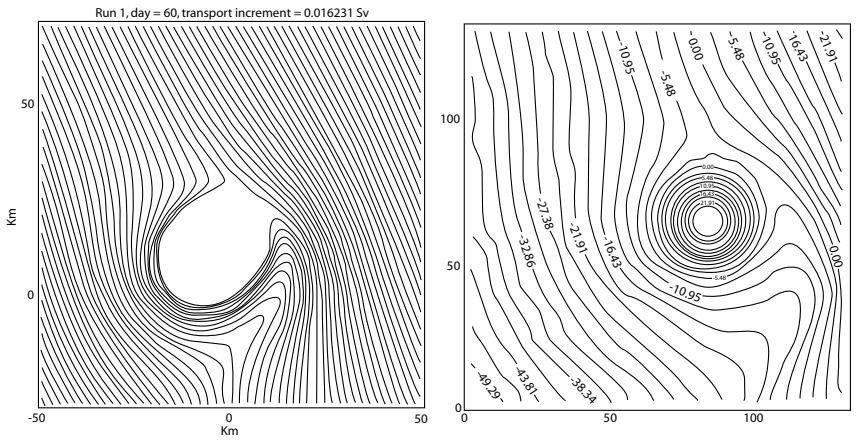

Fig. 6. Streamlines (viewed from the moving eddy) for our first numerical experiments (left-hand side) and a corresponding laboratory experiment of FE (right-hand side). Although the detachment points cannot be seen due to either numerical (our case) or actual mixing (FE case), a region of weak flow is identified in the lee. Also, the noted asymmetry in the direction perpendicular to the migration indicates some friction-induced lift (neglected in our analytical calculation) which forces the eddy to migrate in the NNW direction, instead of directly due north. (Adapted from Flór and Eames, 2002, fig. 6d.)

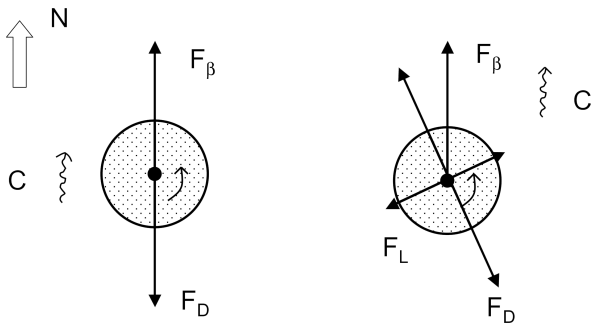

Fig. 7. Schematic diagram of the balance of forces with (right-hand side) and without lift (left-hand side). For the lift to exist some orbital motions from the eddy' core must be transmitted (via friction) to the outer fluid. Since the eddy motions along the rim are small, this transmittal is expected to be small and negligible (left-hand panel). In reality, however, there will be some orbital motion transmission and, in the case of a cyclone in the northern hemisphere, the orbital motions will speed up the outer fluid motions in the west and slow them down in the east giving rise to a westward lift. This lift forces the eddy migration to tilt in the NNW direction so that the β-force will have a component balancing the lift (right-hand panel). It is expected that, relative to the northward β-force, the westward lift will be small for intense eddies and large in the weak eddies case.

5. Summary and discussion

We derived a simple analytical formula for very fast meridional migration rates of intense barotropic eddies. The main balance of forces is conceptually analogous to that associated with the so-called 'terminal velocity' of falling objects where the gravitational force balances the form-drag with the lift playing secondary role (Fig. 7). Here, the β-force balances the form-drag. Observations suggest that most eddies probably do not have a barotropic component as it is quickly (10–100 d) dissipated by bottom friction. It is expected that eddies that do possess a barotropic component probably do so for only a relatively short time after their formation. Assuming that this bottom-driven dissipation is scaled as,

$$H\frac{\mathrm{d}u}{\mathrm{d}t} : C_D u^2, \tag{12}$$

and that $C_D \sim 3 \times 10^{-3}$, $U \sim 0.2$ ms^{-1} and $H \sim 4000$ m, we find that the dissipation time is roughly 75 d.

In this scenario, eddies with barotropic component will move primarily meridionally during the first 75 d (or so) of their lifetime. For Agulhas rings, this agrees with the observations of high northward speeds (Fig. 1) and the presence of a barotropic component. As mentioned, their migratory speeds cannot be explained by neither Sverdrup advection nor bottom topography. Our migration speed formula, $\left(\frac{3\pi}{5}\beta V_{\max}\right)^{1/2} r_{\max}$, on the other hand, suggests that these rings (with a $V_{\max}$ of 0.2 m s^{-1} and an $r_{\max}$ of, say, 40 km, see e.g. Arhan et al., 1999; Boebel et al., 2003) will propagate towards the equator at a rate of 11 cm s^{-1} or 9 km d^{-1}. The formula is also in agreement with the (cyclonic) observation that Fig. 1 displays but, as mentioned, this application is speculative in nature because we have no evidence that the cyclone had a barotropic component. The cyclone in the North Atlantic (Fig. 1) had a similar orbital speed to that of Agulhas rings but was considerably smaller. Taking $r_{\max}$ to be 30 km instead of 40 km, and the same orbital speed of 0.2 m s^{-1}, we obtain a northward migration rate of about 7 km d^{-1}.

Overall, when our numerical experiments are compared to numerical experiments performed by others and to the laboratory experiments of FE, the results are certainly satisfactory. Also, relative to the numerical speeds as well as the laboratory

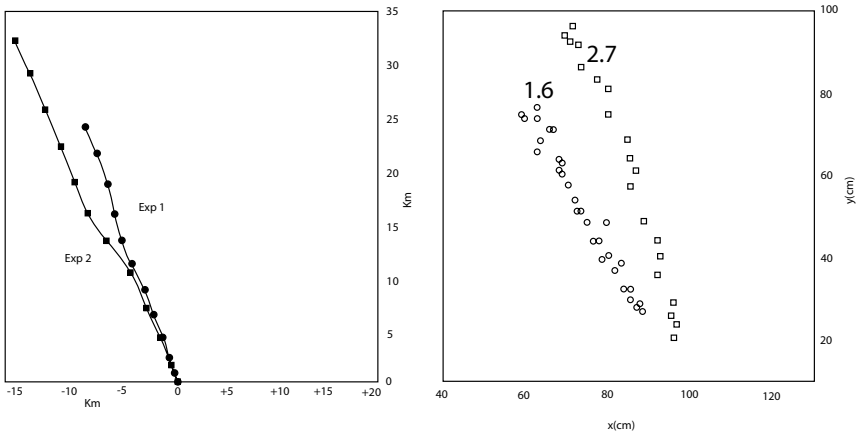

Fig. 8. (Left-hand panel): The trajectory of the eddy centre (maximum relative vorticity) for experiment 1 and 2. For cosmetic reasons, the centre position is calculated daily and then filtered with an 11 d centred running mean. Solid black dots are plotted every 10 d starting at $t = 0$. (Right-hand panel): The analogous laboratory experiments of FE for two intense eddies; see their fig. 9a (from which this figure was adopted) for the parameters associated with the circles and squares. Note the similarity between our numerics and the laboratory experiments.

experiments (Fig. 4), the analytics always take higher values due to the absence of friction. This is in agreement with simple scaling arguments showing that the ratio of the (analytically neglected) frictional forces compared to the β-force [$\sim o(\nu/\beta r^3)$] is roughly 30–50%. The streamlines in the eddy' lee show clear signs of a weakened flow downstream, consistent with the wake idea (Fig. 6). The assumption of relatively small lift (for intense eddies) and, hence, small zonal movements (Fig. 7) is also verified by both our numerical runs and the laboratory experiments of FE (Fig. 8). However, identification of detaching streamlines was impossible due to unavoidable numerical and laboratory mixing which blurs the eddy water with the outer water.

As common for most numerical experiments of this nature (e.g. Simmons and Nof, 2002; Cherubin et al., 2006), we used viscosities corresponding to a diffusion speed ($\nu/\Delta x$) of less than 1 cm s^{-1}. This and the values given in Table 1 are roughly the same as those used by other investigators except in some unusual cases (e.g. Jacobs et al., 1999; Hogan and Hulburt, 2000) where a bit lower values (2 m^2 s^{-1} instead of 3 m^2 s^{-1}) were used. This is because, in contrast to our model that has *only* horizontal friction, these models also include bottom and vertical friction as well as horizontal friction. Our frictional values are, of course, larger than what we wish we could use. These frictional effects reduced the eddy orbital speed, but their importance to the overall balance of forces in the north–south direction is negligible for all the experimental times. The reduction in the orbital speed can be easily seen from the upper panel of Fig. 5 whereas the insignificant role of friction in the force balance can be easily verified by examining the Reynolds number based on the migration speed C.

The Reynolds number measures the ratio of the inertial terms (form-drag in our case) to the horizontal frictional terms which, like brakes, push inward towards the eddy's rim attempting to slow both the orbital speed and the migration speed down. In the *ocean*, it is at least two-orders of magnitude larger than unity indicating that the direct effect of friction on the migration force balance is truly negligible. In the *numerics*, however, the Reynolds number is about three, indicating that the numerical frictional effects are not totally negligible.

The idealized force balance described here is offered as a possible explanation for the rapid transient meridional translation of some eddies; its actual role relative to other factors such as background flow, mutual advection by other eddies, and bottom topography remains to be explored in detail via further analysis of observations and very high-resolution general circulation models.

6. Acknowledgments

We acknowledge the support of the National Science Foundation Grants, OCE-0545204, OCE-0241036 and OPP/ARC-0453846 as well as NASA, NAG5–10860.

7. Appendix: List of symbols

β	lineral variation on the Corolis parameter with latitude
V_m	maximum orbital speed
r_m	radius where the maximum speed occurs
ψ	stream function
$\hat{h}$	ring central depth
R_Γ	Rossby number
R	eddy radius
C_D	non-dimensional bottom drag-coefficient
h	total thickness
u	and v horizonal velocity components
H	the undisturbed depth
η	free-surface displacement
B	Bernuolli integral
$g\eta$	pressure term

F_D form-drag force
u_r radial velocity
u_θ tangential velocity
q speed along the edge of the vortex
C migration speed (poleward for cyclone, equatorward for anticyclone)
f Corolis parameter
υ viscosity
FE Flór and Eames (2002)

References

Acheson, D. J. 1990. *Elementary Fluid Dynamics*. Clarendon Press, Oxford. pp. 397.

Arhan, M., Mercier, H. and Lutjeharms, J. R. E. 1999. The disparate evolution of three Agulhas rings in the South Atlantic Ocean. *J. Geophys. Res.* **104**(C9), 20987–21005.

Boebel, O., Rossby, T., Lutjeharms, J., Zenk, W. and Barron, C. 2003. Path and variability of the Agulhas Return Current. *Deep-Sea Res II* **50**, 35–56.

Byrne, D. A., Gordon, A. L. and Haxby, W. F. 1995. Agulhus eddies: a synoptic view using Geosat ERM data. *J. Phys. Oceanogr* **25**, 902–917.

Cherubin, L. M., Morel, Y. and Chassignet, E. P. 2006. Loop Current ring shedding: the formation of cyclones and the effect of topography. *J. Phys. Oceanogr.* **36**, 569–591.

Clement, A. C. and Gordon, A. L. 1995. Absolute velocity field of Agulhas eddies and the Benguela Current. *J. Geophys. Res.* **100**, 22591–22601.

DeMaria, M. 1985. Tropical cyclone motion in a nondivergent barotropic model. *Mon. Wea. Rev.* **113**, 1199–1210.

Dewar, W. K. and Gailliard, C. 1994. The dynamics of barotropically dominated rings. *J. Phys. Oceanogr.* **24**, 5–29.

Dewar, W. K. and Morris, M. Y. 2000. On the propagation of baroclinic waves in the general circulation. *J. Phys. Oceanogr.* **30**, 2637–2649.

Drijfhout, S. S. 2003. Why anticyclones can split. *J. Phys. Oceanogr.* **33**, 8, 1579–1591.

Firings, E. and Beardsley, R. C. 1978. The behavior of a barotropic eddy on a beta-plane. *J. Phys. Oceanogr.* **6**, 57–65.

Flierl, G. R. 1984. Rossby wave radiation from a strongly nonlinear warm eddy. *J. Phys. Oceanogr.* **14**, 47–58.

Flierl, G. R. 1987. Isolated Eddy Models in Geophysics. *Annu. Rev. Fluid Mech.* **19**, 493–530.

Flór, J. B. and Eames, I. 2002. Dynamics of monopolar vortices on a topographic beta-plane. *J. Fluid Mech.* **456**, 353–376.

Hogan, P. J. and Hulburt, H. E. 2000. Impact of upper ocean-topographical coupling and isopycnal outcropping in Japan/East Sea Models with 1/8° to 1/64° resolution. *J. Phys. Oceanogr.* **30**, 2535–2561.

Ivanov, A. F. and Pramonov, A. N. 1980. In Sinopticheskie vikhri v okeane (Sypnotic Eddies in the Ocean), Naukova Dumka, Kiev, 107–114.

Jacobs, G. A., Hogan, P. J. and Whitmer, K. R. 1999. Effects of eddy variability on the circulation of the Japan/East sea. *J. Oceanogr.* **55**, 247–256.

Kamenkovich, V. M., Koschlyakov, V. N. and Monin, A. S. 1986. *Synoptic Eddies in the Ocean*, Reidel, Dordrecht, Holland, 433.

Kamenkovich, V. M., Leonov, Y. P., Nechaev, D. A., Byrne, D. A. and Gordon, A. L. 1996. On the influence of bottom topography on the Agulhas eddy. *J. Phys. Oceanogr.* **26**, 6, 892–912.

Killworth, P. D. and Blundell, J. R. 2004. The dispersion relation for planetary waves in the presence of mean flow and topography: II. Two-dimensional examples and global results. *J. Phys. Oceanogr.* **35**, 2110–2133.

Korotaev, G. K. 1997. Radiating vortices in geophysical fluid dynamics. *Surv. Geophys.* **18**, 567–619.

McCartney, M. S. and Woodgate-Jones, M. E. 1991. A deep-reaching anticyclonic eddy in the subtropical gyre of the eastern South Atlantic. *Deep-sea Res.* **38**, Supplement 1, S411–S443..

Mied, R. P. and Liendeman, G. J. 1979. The propagation and evolution of cyclonic Gulf Stream rings. *J. Phys. Oceanogr.* **9**, 1183–1206.

Nof, D. 1983. On the migration of isolated eddies with application to Gulf Stream rings. *J. Mar. Res.* **41**, 399–425.

Nof, D. 1985. Joint vortices, eastward propagating eddies and migratory Taylor columns. *J. Phys. Oceanogr.* **15**, 1114–1137.

Nof, R. and Simon, L. 1987. Laboratory experiments on the merging of anticyclonic eddies. *J. Phys. Oceanogr.* **17**, 343–357.

Olson, D. B. and Evans, R. J. 1986. Rings of the Agulhas. *Deep-Sea Res.* **33**, 27–42.

Paldor, N., Rubin, S. and Mariano, A. J. 2007. A consistent theory for linear waves of the shallow water equations on a rotating plane in mid-latitudes. *J. Phys. Oceanogr.* **37**(1), 115–128.

Pichevin, T., Nof, D. and Lutjeharms, J. 1999. Why are there Agulhas Rings?. *J Phys. Oceanogr.* **29**, 693–707.

Reznik, G. M., Grimshaw, R. and Benilov, E. S. 2000. On the long-term evolution of an intense localized divergent vortex on the beta-plane. *J. Fluid Mech.* **422**, 249–280.

Robinson, A. R. 1983. *Eddies in Marine Science*. Springer-Verlag, Berlin Heidelbeg, 609.

Rossby, C. G. 1948. On displacements and intensity changes of atmospheric vortices. *J. Mar. Res.* **7**, 175–187.

Schmid, C., Boebel, O., Zenk, W., Lutjeharms, J. R. E., Garzoli, S. L., Richardson, P. L. and Barron, C. 2003. Early evolution of an Agulhas Ring. *Deep-Sea Res.* **50**(1), 141–166.

Simmons, H. and Nof, D. 2002. The squeezing of eddies through gaps. *J. Phys. Oceanogr.* **32**, 314–335.

Smith, R. B. 1993. A Hurricane Beta-Drift Law. *J. Atmos. Sci.* **50**, 3213–3215.

Schouten, M. W., De Ruijter, W. P. M., van Leeuwen, P. J. and Lutjeharms, J. R. E. 2000. Translation, decay and splitting of Agulhas rings in the south-east Atlantic ocean. *J. Geophys. Res.* **105**, 21 913–21 925.

Van Aken, H. M., van Velthoven, A. K., Veth, C., De Ruijter, W. P. M., Van Leeuwen and co-authors. 2003. Observations of a young Agulhas righ, Astrid, during MARE in March 2000. *Deep-Sea Res. II* **50**, 167–195.

Witter, D. L. and Gordon, A. L. 1999. Interannual variability of South Atlantic circulation from four years of TOPEX/POSEIDON satellite altimeter observations. *J. Geophys. Res.* **104**, 20 927–20 948.